Journal of Radioanalytical and Nuclear Chemistry (2019) 321:791–803
https://doi.org/10.1007/s10967-019-06662-y

Preparation and characterization of a novel diatomite-based composite and investigation of its adsorption properties for uranyl ions

Zeynep Mine Şenol[1] · Dilek Şenol Arslan[2] · Selçuk Şimşek[3]

Received: 18 April 2019 / Published online: 20 July 2019

Abstract
In this research, Polyacrylamide-diatomite (PAA-D) composite was used as adsorbent for the efficient removal of uranyl ions from aqueous solution. The chemical and morphological properties of PAA-D composite were confirmed by several analysis. Batch experiments were performed as a function of solution pH, initial concentration, kinetic, thermodynamic and recovery. The maximum metal uptake capacity was found as 0.085 mol kg^{-1}. Kinetic data were best interpreted by a pseudo second order model. Thermodynamic findings showed that the adsorption process was exothermic, spontaneous and process with increased disorderliness at solid/solution interface. The recovery studies showed that PAA-D composite had good adsorption/desorption performance.

Keywords Diatomite · Uranyl · Composite · Polyacrylamide · Adsorption

Introduction

Rapid developments of nuclear technology as well as the mixing metal specimens used in these areas to the environment and water as a waste poses a serious threat to environment and human health. Uranium is a radioactive element, is mainly used in nuclear facilities with its highly enriched form, while low enriched uranium is used in widely range of military, industrial and scientific purposes [1]. So, wastes generated by this widespread use of uranium has a major impact on human health and environment. A recent study by Wang et al. [2] concluded that the most common type of uranium in aqueous phase is hexavalent uranium (UO_2^{2+}), which has a radioactive property. It accumulates in organs such as bone, liver and kidney and it's the leading cause of cancer deaths and organ failure. In addition, the recovery of rare precious metals from waste is economically important. For example the concentration of uranium in seawater was measured approximately 3.3 μgL^{-1}, and considering this amount, recovery studies are the most important [3].

With these properties, the recovery of uranium from the environment by various methods has become one of the most investigated species. Adsorption is the one of the most effective method for the recovery or removal from the species, which found as pollutants. This method compared with other commonly used methods for example, precipitation [4], filtration [5], biological treatment [6] it comes into prominence with its easy applicability, development of selective adsorbent for related species and economical.

Synthetic polymers [7], minerals [8, 9], natural polymers [10], and composites [11, 12] which can carry a functional group and complex with metals, or can be used for metal adsorption by ion exchange, are widely used especially in the removal of metal contaminants [4]. Natural minerals, such as clay, zeolite, sepiolite, diatomite, have been found to be potentially absorptive because of their high surface area and being open to modification and [13]. However, a number of undesirable properties of these natural minerals, such as surface loads, alterations of pH solution or coagulation, have made it difficult to use them in various modifications or composites.

✉ Selçuk Şimşek
simsek@cumhuriyet.edu.tr

[1] Department of Food Technology, Zara Vocational School, Cumhuriyet University, 58140 Sivas, Turkey

[2] Materials Science and Nanotechnology Engineering Department, Engineering Faculty, Abdullah Gül University, Kayseri, Turkey

[3] Department of Chemistry, Faculty of Science, Cumhuriyet University, 58140 Sivas, Turkey

Diatomite is a silicate rock which has high surface area formed by fossilized skeletons of unicellular algae [14]. Studies have shown that, diatomite is a potential adsorbent for pollutants which is a natural material with high water holding capacity [15]. However, coagulation with water limits the practical use of diatomite as an adsorbent.

In this research, a novel composite was formed by using diatomite and polyacrylamide hydrogel which is known as inert and has a high water holding capacity. Thus, the adsorption of uranyl ions in the aqueous phase using this composite as the adsorbent was aimed. The characterization of the new composite was illuminated by FT-IR, SEM, EDX and surface load surveys. The parameters affecting the adsorption of the uranil ion have been investigated in terms of pH, initial concentration, time, temperature and recovery. The results showed that the new composite formed can be used as an effective adsorbent for uranyl ion by means of its economicalness, ease of composite formation, high adsorption capacity and adsorption rate.

Experimental procedure

Reagents and instrumentation

Diatomite used in the adsorption research was obtained from Akmin Mining (Ankara). Ammonium persulphate (APS), Acrylamide monomer (AA), N,N,N′,N′-tetramethylenediamine (TEMED) and N,N′-methylenebisacrylamide were purchased from Sigma (St. Loius, MO, USA). $(CH_3COO)_2UO_2{\cdot}2H_2O$ and 4-(2-pyridilazo) resorcinol (PAR) as complexing agent in spectrophotometric measurements of uranly ion and other chemicals were purchased from Merk (Germany). Ultrapure water was used in all experiments. All experiments were continuously double run. PAA-D and its components were characterized by FT-IR, SEM–EDX (TESCAN MIRA3 XMU) and XRD (RIGAKU) analysis. FT-IR analysis was recorded using the FT-IR spectrophotometer (Perkin Elmer 400) in order to examine the functional groups in the range of 400–4000 cm^{-1} with KBr pellets. The specific surface area and micropore volume of diatomite (D) and polyacrylamide-diatomite (PAA-D) composite were measured using N_2 adsorption–desorption (AUTOSORB 1C) at − 196 °C. The surface area, total pore volume and micropore volume were determined by multipoint BET (Brunauer, Emmett and Teller), t-plot and DR (Dubinin–Radushkevic), respectively. Uranyl concentration was determined using UV–VIS spectrophotometer (SHIMADZU, 160 A model, Japan). This spectrophotometer has a wavelength range of ± 0.2 nm and 2 nm wavelength within the range of 190–1100 nm. A pH meter (Selecta, Spain) was used to measure pH values with glass-calomel electrodes. Centrifuge (Hettich Universal) was used to accelerate phase separation. A thermostatically controlled water bath to keep the constant temperature (Nuvent 120, Turkey) was used.

Synthesis of composite

For synthesis of PAA-D composite, 1 g of diatomite in 20 mL of distilled water and 20 mL of solution containing 2 g acrylamide monomer were stirred until a homogenous mixture was obtained. Then 0.2 g N,N′ methylenebisacrylamide was added onto this mixture and stirred on magnetic stirer. Polymerization reaction was sustained by adding 400 µL of N,N,N′,N′-tetramethylenediamine (TEMED) and 1 g ammonium persulfate (APS) in rapid cycle. The obtained new composite was washed with ultrapure water for several times in order to reach approximately pure water conductivity. After then, it was dried at 40 °C, ground (50 mesh), stored in an airtight container.

Batch adsorption procedure

Adsorption experiments were carried out using batch method. The adsorbent–solution systems where equilibrated with 1000 mg L^{-1} (3.7×10^{-3} mol L^{-1}) uranyl concentration at pH 4.5, for 24 h at 298 K in a 10 mL polypropylene tubes. The concentration of uranyl ions was determined by using the PAR method [16]. In this method, concentration of UO_2^{2+} ions are formed as spectrophotometrically a selective complex with PAR at $\lambda = 530$ nm. %Adsorption and Q (mol kg^{-1}) values shown in Eqs. 1 and 2;

$$\%\text{Adsorption} = \left[\frac{C_i - C_f}{C_i}\right] \times 100 \quad (1)$$

$$Q = \left[\frac{C_i - C_f}{m}\right] \times V \quad (2)$$

Here, C_i; the initial concentration of the adsorbed (mg L^{-1}), C_f; equilibrium concentration (mg L^{-1}), Q (mol kg^{-1}) the amount of adsorbed ions, m; the adsorbent mass (g) and V define the solution volume (L). The synthesis of PAA-D composite and batch adsorption process is presented in Fig. 1.

Reusability procedure

Under the optimized conditions, the reusability availability of PAA-D for UO_2^{2+} adsorption were desorbed from the adsorbent using 10 mL of 1 M HCl, HNO_3, NaOH and Ethyl alcohol. The desorbed amount of uranyl was determined by spectrophotometric method.

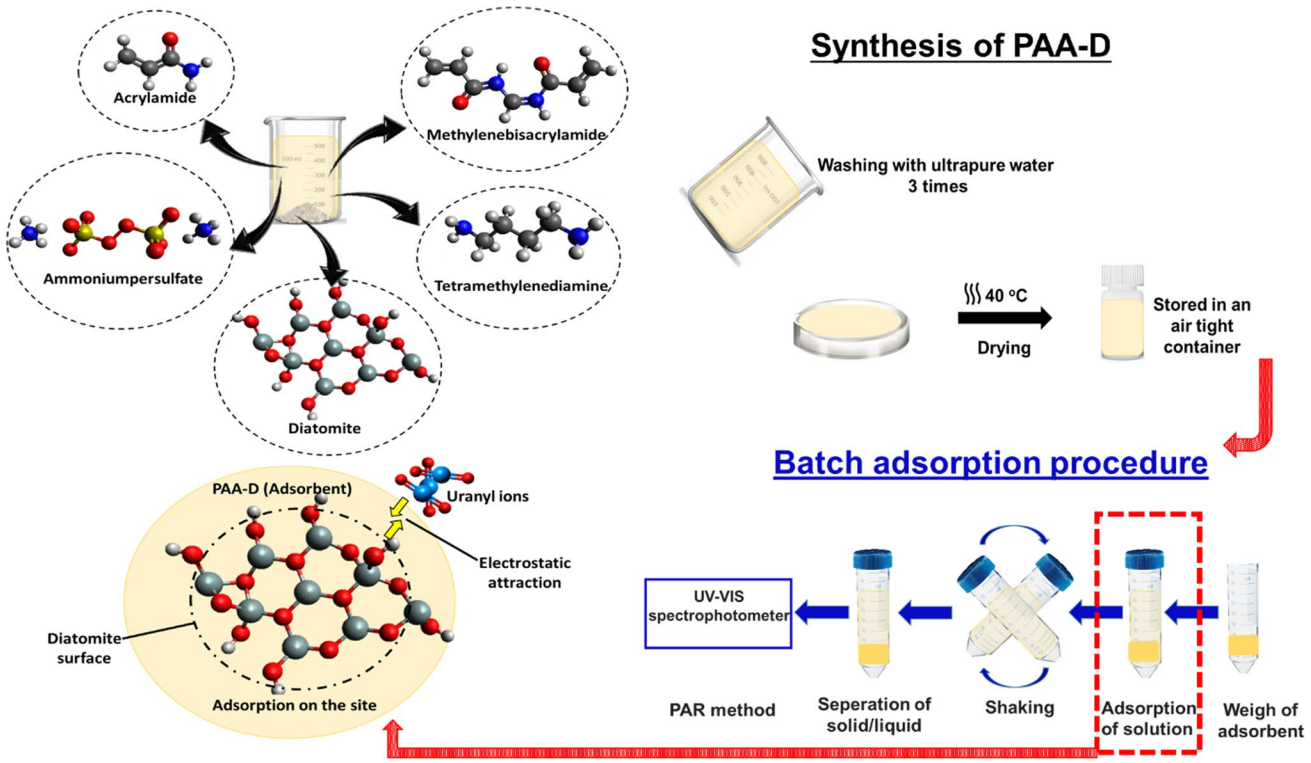

Fig. 1 Schematic illustration for synthesis of PAA-D composite used as the adsorbent for the removal of uranyl ions from aqueous solution and batch adsorption process

Results and discussion

SEM/EDX investigation results

The SEM images of D, before, and after the adsorption of UO_2^{2+} on PAA-D were shown in Fig. 2a, b, c. The Fig. 2a clearly reveals that the well-preserved forms of diatoms generally have cylindrical and disk shapes with well-developed porous structure. There are also small broken particles of other kinds of diatoms [17]. The SEM image of PAA-D shows a structure having the morphology of the component in Fig. 2b. Figure 2c shows that the surface morphology changed when porous surface adsorbed UO_2^{2+}. Figure 2d shows the EDX results of after adsorption of UO_2^{2+} on PAA-D. As seen from these results, the PAA-D is consisted with elements of O (40.86%), C (21.00%), Si (12.93%), Mg (10.23%), U (5.98%), Al (4.66%) and Fe (4.34%). The C and O contents of PAA-D is evidence of presence of PAA. On the other hand, the U content of PAA-D is evidence of adsorption of UO_2^{2+} on PAA-D.

FT-IR analysis results

The Fourier transform infrared spectroscopy (FT-IR) analysis is utility technique used to obtain an infrared spectrum of metal absorption of the functional groups. D and PAA-D were characterized by FT-IR spectrophotometer (Fig. 3). In the FT-IR spectrum of D is observed peaks for asymmetric stretching of Si–O–Si bonds at 1076 and 1100 cm^{-1}, the peaks symmetric stretching of SiO–H bonds at 750 and 850 cm^{-1} and Si–O–Si bonding vibration at 493 cm^{-1} [17–20]. In the PAA-D spectrum is observed peaks representing the –C=O stretching vibration of the amide group at 1672 cm^{-1}, the $–NH_2$ bending vibration of the amide group at 1610 cm^{-1}, the –CN stretching vibration of the amide group at 1425 and 700 cm^{-1} in structures of the PAA [21, 22]. These results showed that the PAA-D composite was successfully synthesized.

When the FTIR spectrum of the uranyl adsorbed PAA-D structure is examined, it is observed that peaks 678, 1176 and 1348 cm^{-1} are formed after adsorption. The increased intensity of peak at 712 cm^{-1} in PAA-D structure after adsorption and the shift in peak maximum wavelength were considered as evidence of uranium entering the structure.

XRD analysis

Figure 4 shows the divergence among the used diatomite in calcined form, polyacrylamide (PAA) modified diatomite composite and UO_2 doped PAA-D composite in powder form. Pure diatomite (XRD-PDF #33-1161) can be seen characteristic by a hump at 22° 2θ with some trace phases

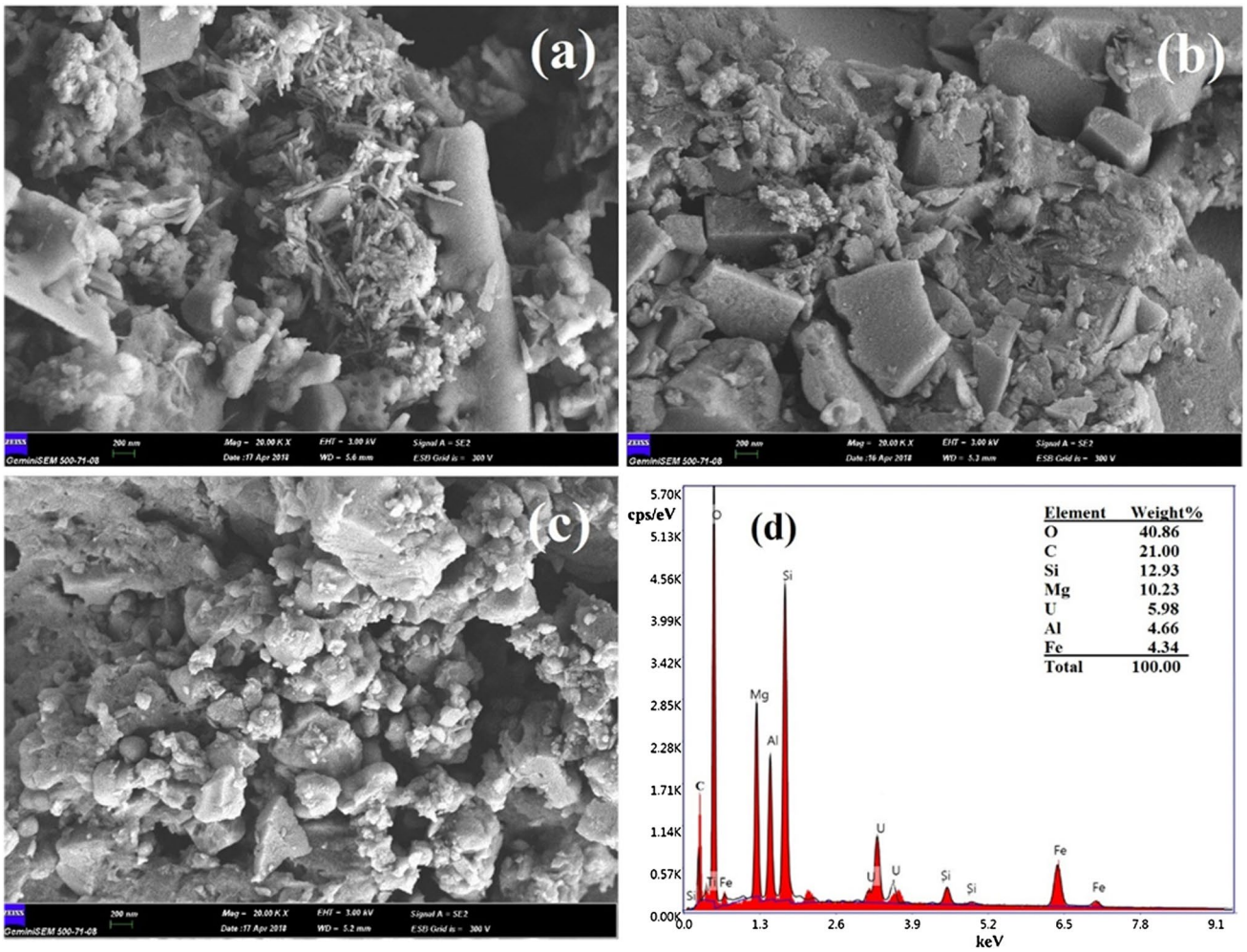

Fig. 2 SEM images of D (**a**), PAA-D, before adsorption of UO_2^{2+} (**b**), PAA-D, after adsorption of UO_2^{2+} (**c**), EDX pattern obtained the after adsorption of UO_2^{2+} (**d**) {$[UO_2^{2+}]_0$: 1000 mg L^{-1}, adsorbent dosage: 100 mg, natural pH: 4.0–4.5, contact time: 24 h, temperature: 298 K}

of calcite (CaO) and silicate (quartz-SiO_2) as seen by narrow sharp peaks as 28° and 29° 2θ. This can be attributed to the opal form ($SiO_2 \cdot nH_2O$) of diatomite, which transformed into quartz, after dehydration by the calcination. Many other small peaks are evident due to dehydrated layered silicates forming a monoclinic and triclinic large non-symmetric crystal [23].

The presence of polymer phase in PAA-D composite can be seen by the hedged top of main diatomite peak around 22°, can be seen by the hedged top of main diatomite peak around 22° 2θ to form a amorphous hump which is characteristic for polymers. Same trace compounds as calcite and silicate can still be seen as intercalated by polymer between layers mainly due to the enlarged peak at 29° [24].

The presence of UO_2 in PAA-D composite can clearly be identified by the increased peaks at 28° and 32° 2θ as main two peaks of UO_2 (XRD-PDF #75-0420) accompanied by 47° and 56° 2θ as other strong diffractions. By the addition of U cation into the PAA-D composite, the sharp peak of diatomite can be seen again at 22° while the quartz peak was disappeared at 29° [25, 26]. This may be due to the deterioration of layered structure of silicate due to the symmetric UO_2 cubic crystal may affect Si cation as a crystal stabilizer. The average yield of UO_2 in PAA-D composite can be approximated ranged from 7 to 10 wt% in dry basis as calculated due to peak intensity and peak area measurements, respectively by post process in XRD MDI Jade® program.

BET analysis

Nitrogen adsorption–desorption isotherms of D and PAA-D and the results of BET analysis were given in Fig. 5 and Table 1, respectively. According to IUPAC, if the pore diameter of the materials is in the range of 2–50 nm and > 50 nm the mesopore and macropore are defined, respectively. On the other hand, if the pore diameter is < 2 nm, the structure

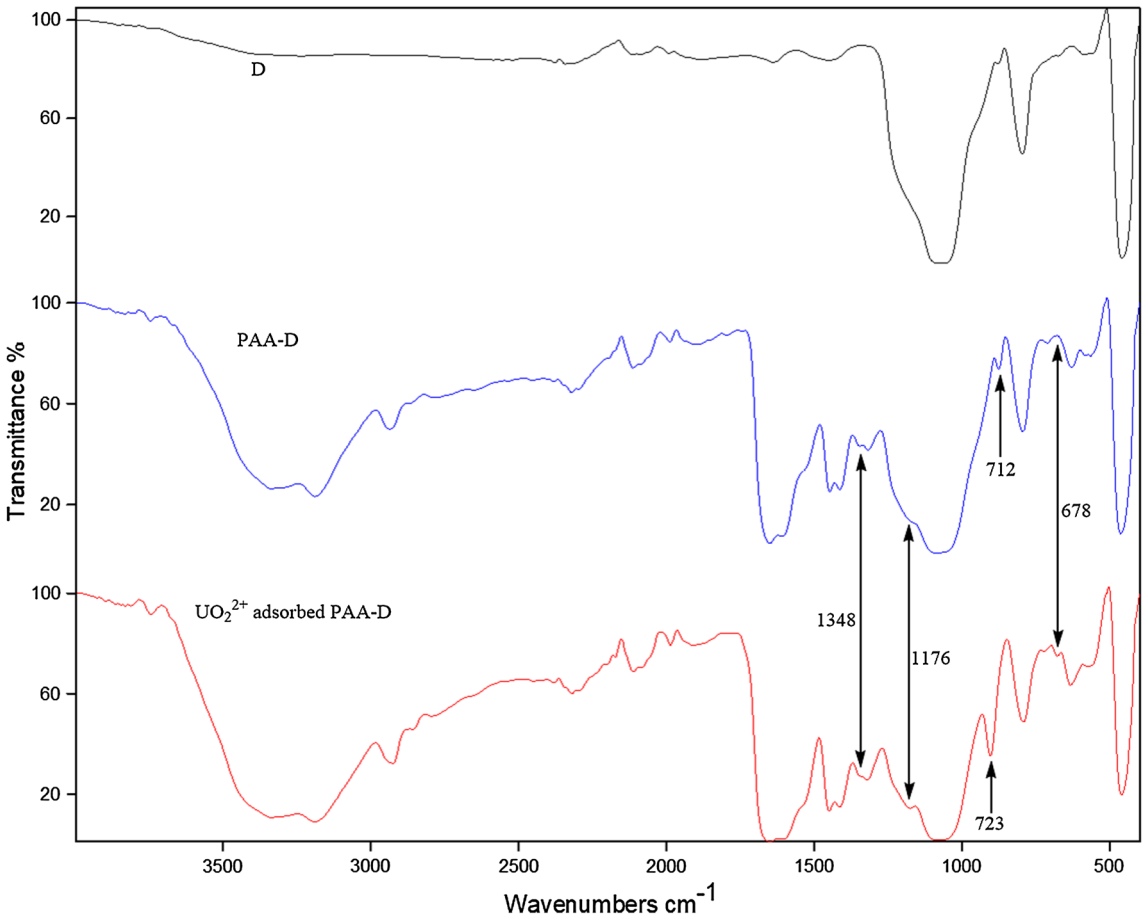

Fig. 3 FT-IR spectrum of D, PAA-D and UO_2^{2+} adsorbed PAA-D {$[UO_2^{2+}]_0$: 1000 mg L^{-1}, adsorbent dosage: 100 mg, natural pH: 4.0–4.5, contact time: 24 h, temperature: 298 K}

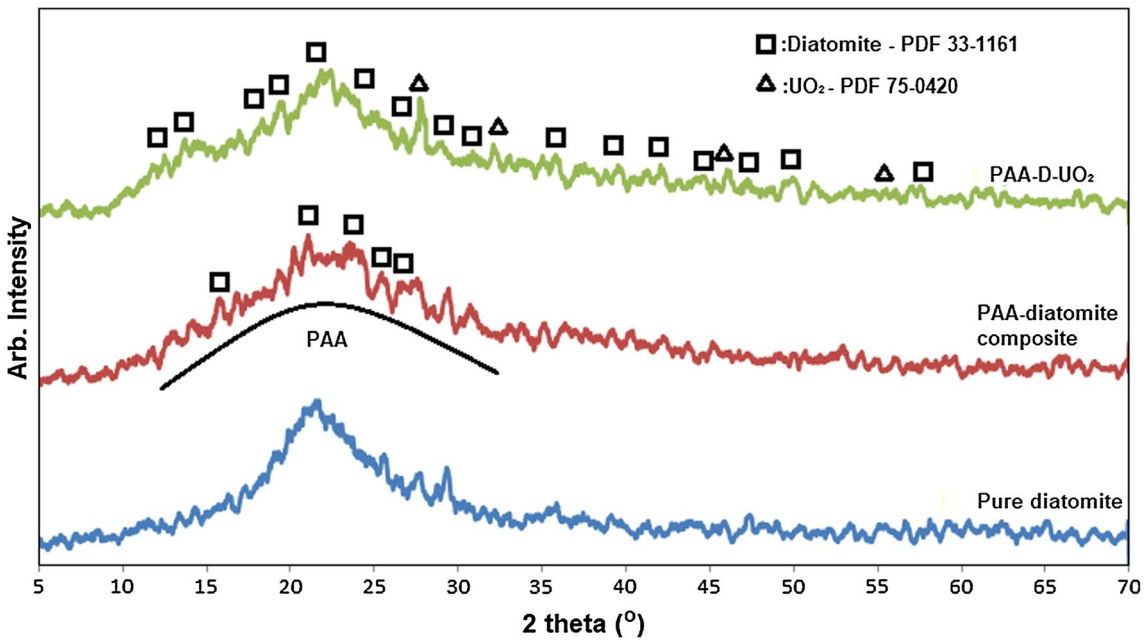

Fig. 4 XRD spectra of D and PAA-D

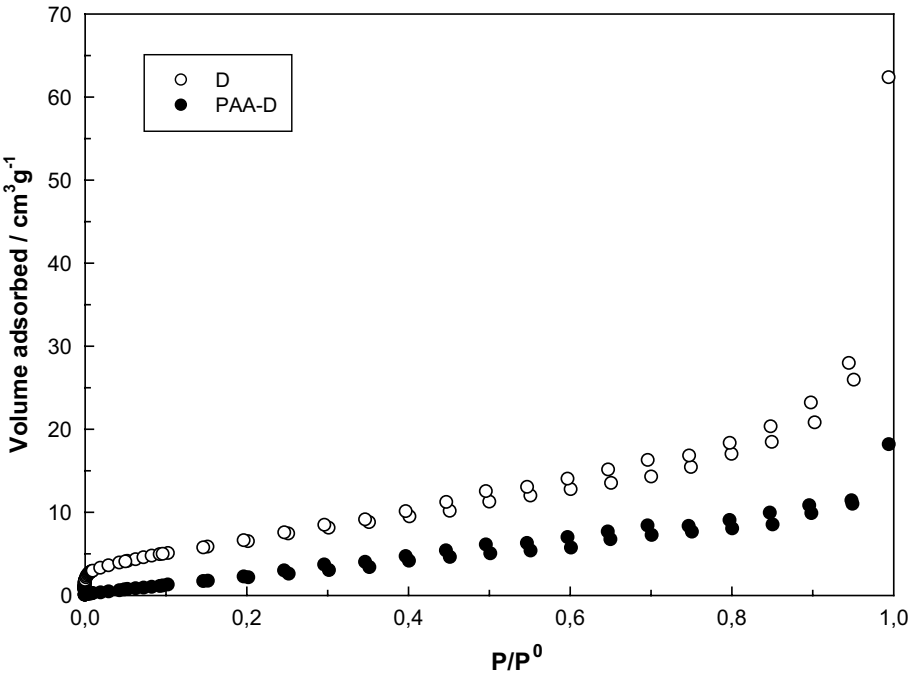

Fig. 5 Nitrogen adsorption–desorption isotherms of D and PAA-D

Table 1 Changes in specific surface area and pore characteristics of D and PAA-D

Sample	S^{a}_{BET} ($m^2\ g^{-1}$)	V^{b}_{Total} ($cm^3\ g^{-1}$)	V^{c}_{micro} ($cm^3\ g^{-1}$)	D_p (Å)
D	51.8	0.1035	0.00914	7.80
PAA-D	21.5	0.0333	0.00320	4.27

[a]Multipoint BET method

[b]Volume adsorbed at $p/p_0 = 0.99$

[c]Micropore volume calculated by DR method

is defined as microporous [27]. When Table 1 was examined, it is seen that the porous diameter of D and PAA-D were < 2 nm, which indicates that D and PAA-D have a microporous structure. The pore size of the PAA-D composite was found to be less than D. It is thought that, the decrease in pore size after the formation of the composite structure may be due to the narrowing of the pores due to the filling of the polyacrylamide pores. As shown in Table 1, PAA-D was reduced the BET surface area, pore volume and pore diameter compared to D.

Effect of solution pH

One of the most important parameters affecting the adsorption process of metal ions is the pH of aqueous solution. This situation is directly related to the competition abilities of hydrogen ions with the metal ions to the active sites of absorbent. Adsorbent surface is protonated at low pHs, therefore the interaction between the surface and the ions is decreased, so adsorption reduces. Hydrogen ion concentration decreases with increasing pH and the amount of adsorbed metal increases.

The pH effect of adsorption of UO_2^{2+} ions on PAA-D was studied in the pH range 1–7. The results clearly shown that, the adsorption rate increased with increasing pH (Fig. 6).

It was observed that adsorption increased from 19 to 91% by increasing pH from 1 to 7. The maximum adsorption was reached 91% at pH 6. As the concentration of H^+ ions decreased, the amount of adsorbed UO_2^{2+} was increased with increasing pH. Hydrolysis of uranium ions increases with increasing pH. For these reason, the values above pH 6 has not been overpassed due to hydroxide precipitates of the UO_2^{2+} ions for example $(UO_2)_3(OH)^{7-}$, $UO_2(OH)^{3-}$, $UO_2(CO_3)_3^{4-}$ precipitates [28, 29].

The determination of point of zero charge (PZC) was perform to examine the surface charge and acidic–basic character of adsorbent. For that 0.1 g PAA-D and D were prepared and their initial pH was adjusted in the range of 1.0–12.0 by NaOH and HCl at 298 K for 24 h and results shown in Fig. 7. The surface charge of D and PAA-D were found 7.1 and 4.9 respectively. Therefore, the surface of PAA-D composite adsorbent above pH 4.9 is negatively charged, under these values it is positively charged. The decreasing adsorption of UO_2^{2+} ions on PAA-D at low pHs explained in terms of changing in the surface charge of the adsorbent.

Adsorption isotherm models

Modeling of equilibrium data in adsorption studies is most important for to evaluate adsorbents in terms of adsorption capacity. The experimental data were applied to the

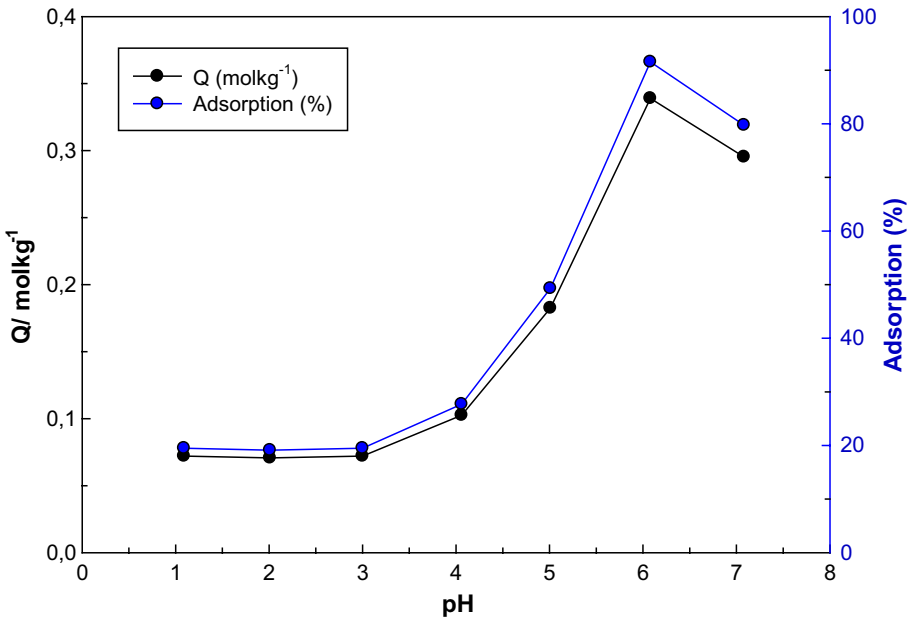

Fig. 6 The effect of pH on the adsorption {$[UO_2^{2+}]_0$: 1000 mg L^{-1}, adsorbent dosage: 100 mg, pH:1.0–7.0, contact time: 24 h, temperature: 298 K}

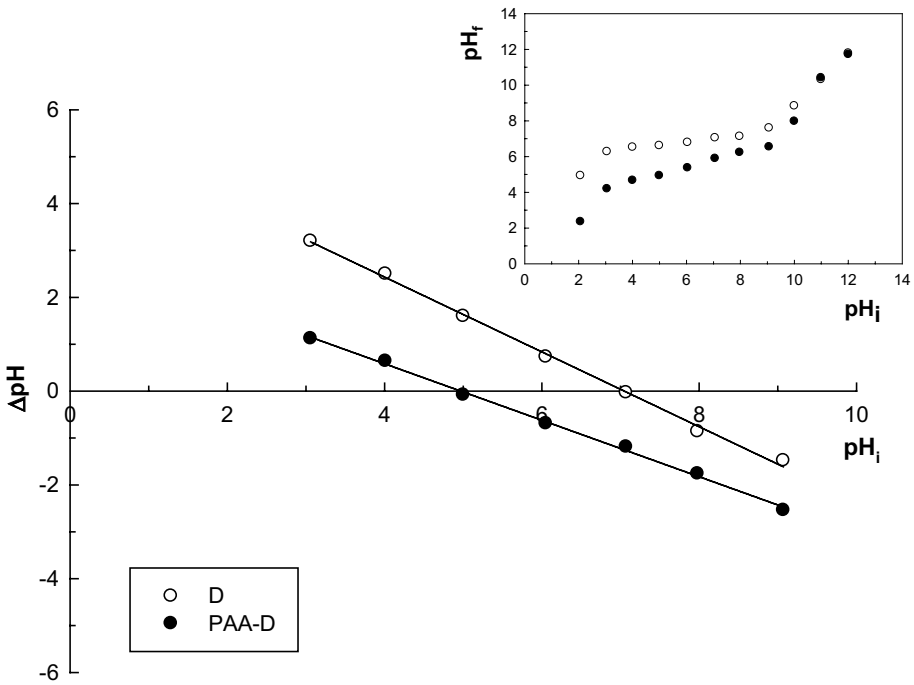

Fig. 7 PZC plots of D and PAA-D

Langmuir, Freundlich and Dubinin–Radushkevich isotherm models and the related parameters were derived.

The Langmuir isotherm model is used successfully in monolayer adsorption processes and assumes that adsorption is homogeneous in active centers on the adsorbent. This model can be written in non-linear form Eq. 3 [30].

$$Q = \frac{K_L X_m C_e}{1 + K_L C_e} \quad (3)$$

X_m Langmuir monolayer adsorption capacity (mol kg^{-1}), K_L Langmuir adsorption equilibrium constant (L mol^{-1}), C_e Equilibrium concentration. Figure 8 shows the compability to the Langmuir, Freundlich and Dubinin–Radushkevich isotherm models and Table 2 shows the parameters derived from all these models. The maximum UO_2^{2+} adsorption capacity for PAA-D was 0.085 mol kg^{-1} and the K_L value was 54,490 L mol^{-1}.

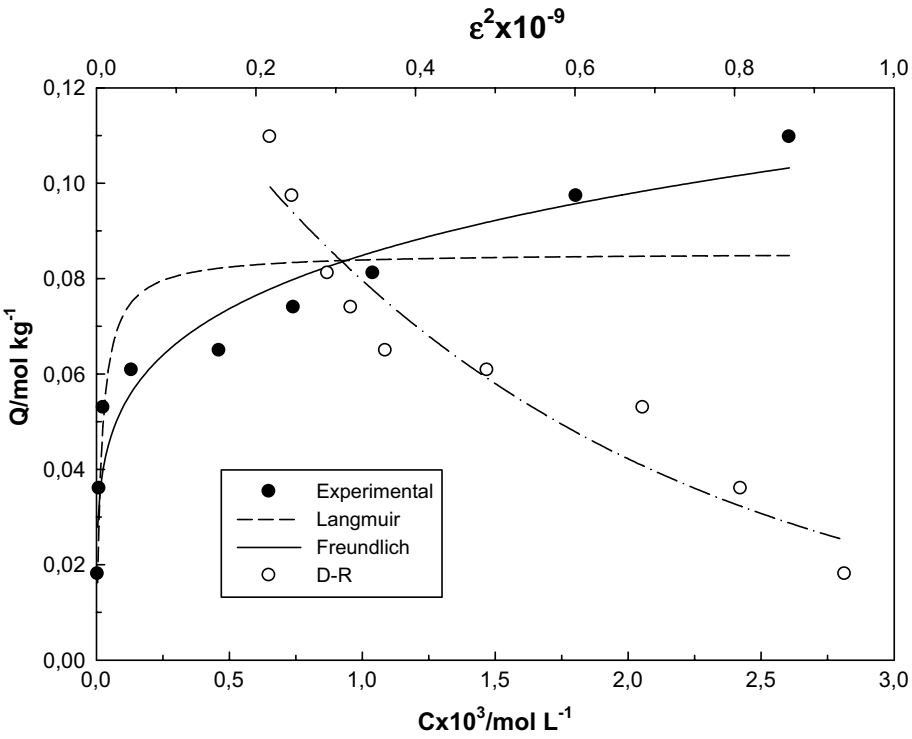

Fig. 8 Experimentally obtained adsorption isotherms UO_2^{2+} and their compatibility to Langmuir, Freundlich and D–R models {$[UO_2^{2+}]_0$: 50–1000 mg L^{-1}, adsorbent dosage: 100 mg, natural pH: 4.0–4.5, contact time: 4 h, temperature: 298 K}

Table 2 Langmuir, Freundlich and D–R models parameters

Langmuir			Freundlich			Dubinin–Radushkevich			
X_m (mol kg^{-1})	K_L (L mol^{-1})	R^2	K_f	β	R^2	X_{DR} (mol kg^{-1})	$-K_{DR}\times10^9$ (mol^2 KJ^{-2})	E_{DR} (J mol^{-1})	R^2
0.085	54,490	0.785	0.348	0.204	0.933	0.15	1.91	16.2	0.919

The nonlinear experimental data of Freundlich isotherm model, which provides information about the heterogeneity of the adsorbent surface, explains the hyperbolic adsorption behavior. The Freundlich equality is given in Eq. 4. [31].

$$Q = K_f C_e^{\beta} \tag{4}$$

K_f a measure of adsorption capacity, β: refers to the surface heterogeneity of the adsorbent. Freundlich isotherm parameter K_f which indicates the capacity of adsorption was found as 0.348 and β refers to the surface heterogeneity of the adsorbent was found as 0.204, which less than one, indicating that the adsorption of UO_2^{2+} ion onto PAA-D is favorable. Comparison of R^2 values between Langmuir and Freundlich isotherm models indicated that the adsorption of UO_2^{2+} ion on PAA-D was better fitted the Freundlich isotherm.

Dubinin–Radushkevich (D–R) model is based on the assumption that the adsorption is related to the surface porosity and pore volume. This model interested in energetic perspective. The D–R equality is given in Eq. 5;

$$Q = X_{DR} e^{-K_{DR}\varepsilon^2} \tag{5}$$

In this equation (Eq. 5); Q (mol kg^{-1}): the amount of adsorbed UO_2^{2+}, X_{DR} a measure of adsorption capacity, K_{DR} (mol^2 KJ^2) activity coefficient, ε Polanyi potential (Polanyi potential is used as if $\varepsilon = RT\ln\left(1+\frac{1}{C_e}\right)$, R the ideal gas constant (8.314 J mol^{-1} K^{-1}), T (K) absolute temperature, E_{DR} adsorption free energy (kJ mol^{-1}) is calculated by Eq. 6.

$$E_{DR} = \left(2K_{DR}\right)^{-0.5} \tag{6}$$

The E_{DR} value indicates the adsorption mechanism, which is a physical or chemical. $8 < E < 16$ indicates that the adsorption is chemically controlled and while $E < 8$ kJ mol^{-1} reveals the adsorption process physically [32, 33]. The compability to the Langmuir, Freundlich and D–R isotherm models were seen in Fig. 8 and the parameters derived from these models were presented in Table 2. E_{DR} value was found as 9.7 kJ mol^{-1}. This means that the adsorption process carried out by chemical ion exchange mechanism.

The change of initial concentration with adsorption and Q (mol kg^{-1}) values shown in Fig. 9. Adsorption% values decreased from 97 to 29% in 50–1000 ppm UO_2^{2+}

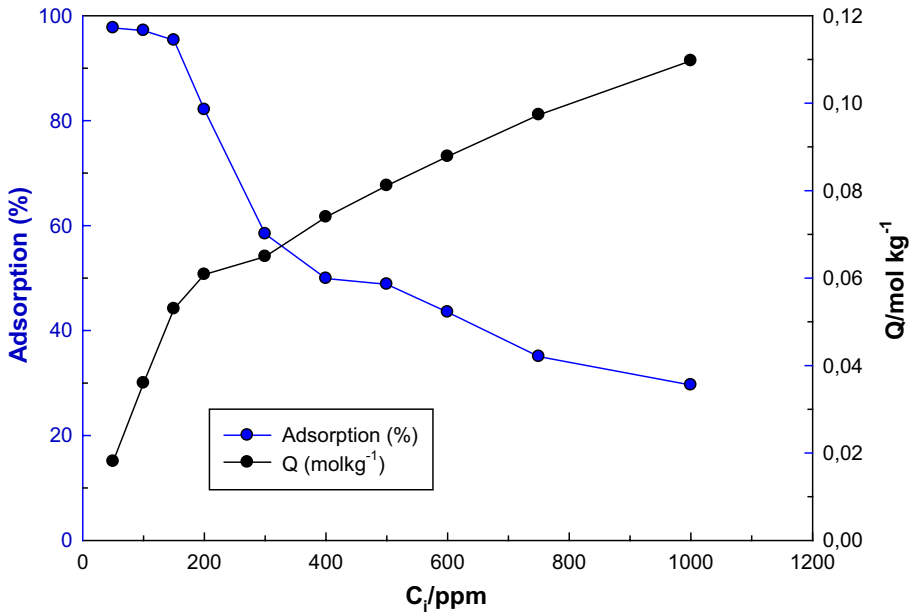

Fig. 9 The effect of concentration on the adsorption {$[UO_2^{2+}]_0$: 50–1000 mg L^{-1}, adsorbent dosage: 100 mg, natural pH: 4.0–4.5, contact time: 24 h, temperature: 298 K}

ion concentration. It was observed that, high adsorption at lower UO_2^{2+} concentration and adsorption decreased with increasing UO_2^{2+} ion concentration. This state clearly indicated that the active adsorption sites on PAA-D was decreased and saturated over the time.

Adsorption kinetics

Determination of kinetic parameters such as selectivity, adsorption capacity, pH is the most important data to understand the mechanism of adsorption. Mainly, significant point is how long does time take to complete the adsorption? For this reason, it must be known that the half-time of adsorption initial rate of adsorption and rate constant of reaction.

Lagergren's pseudo first-order, pseudo second-order and intraparticle diffusion models were applied to description of the adsorption kinetics of UO_2^{2+} ions on PAA-D. Lagergren's pseudo-first-order (Eq. 7); [34]

$$Q_t = Q_e\left(1 - e^{-k_1 t}\right) \tag{7}$$

Q_t (mol kg^{-1}) is the adsorption capacity at time t, Q_e (mol kg^{-1}) is the adsorption/loading capacity at equilibrium, k_1 (min^{-1}) pseudo first-order equilibrium rate constant. Pseudo-second-order (Eq. 8); [35].

$$Q_t = \frac{t}{\left[\frac{1}{k_2 Q_e^2}\right] + \left[\frac{1}{Q_e}\right] t} \tag{8}$$

k_2 (mol^{-1} kg min^{-1}) is the pseudo second-order rate constant. The initial rate for the pseudo-first-order and pseudo-second-order models of adsorption calculated using Eqs. 9 and 10.

$$H_1 = k_1 Q_e \tag{9}$$

$$H_2 = k_2 Q_e^2 \tag{10}$$

Q_t (mol kg^{-1}) the amount of adsorbed ions at t time, Q_e (mol kg^{-1}) the amount of adsorbed ions at equilibrium time, k_1 (min^{-1}) the first order rate constants, k_2 (mol kg min^{-1}) the second order rate constants. Intraparticle diffusion model calculated using Eq. 11 [36, 37]. k_i (mol kg^{-1} $min^{-0.5}$) the intraparticle rate constant.

$$Q_t = k_i t^{0.5} \tag{11}$$

Compatibility of UO_2^{2+} adsorption kinetics graphs to pseudo-first-order model, pseudo-second-order model and intraparticle diffusion models were shown in Fig. 10. Experimental Q_e and theoretically calculated Q_t, kinetic rate constants (k_1, k_2, k_i) and regression coefficients (R^2) were shown in Table 3. According to these studies, harmony of experimental (Q_e) and theoretical (Q_t) data are compatible with the pseudo-second order model as can be seen in Fig. 10. When the R^2 values were examined, it was observed that the adsorption kinetics were compatible with the pseudo-second order model.

Adsorption thermodynamics

The effect of temperature on the biosorption was examined at different temperature values as 278 K, 298 K and 313 K. Thermodynamic parameters including enthalpy change ($\Delta H°$), entropy change ($\Delta S°$) and free energy change ($\Delta G°$) were determined using the following equations; The

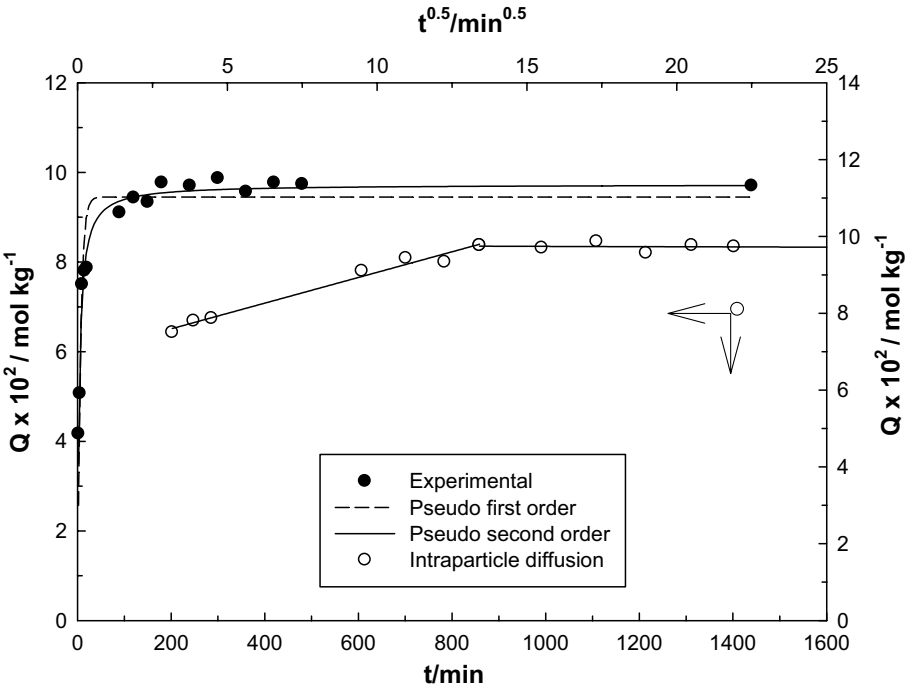

Fig. 10 Compatibility of UO_2^{2+} adsorption kinetics to pseudo-first-order, pseudo-second-order and intraparticle diffusion models {$[UO_2^{2+}]_0$: 1000 mg L^{-1}, adsorbent dosage: 300 mg, natural pH: 4.0–4.5, contact time: 24 h, temperature: 298 K}

Table 3 Pseudo-first-order, pseudo-second-order and intraparticle diffusion models parameters

Q_t/mol kg^{-1}	Q_e/mol kg^{-1}	R^2	$k_1 \times 10^3/dk^{-1}$	$H \times 10^3$/mol kg^{-1} min^{-1}
Pseudo-first-order				
0.089	0.095	0.882	158	15.1
Pseudo-second-order				
Q_t/mol kg^{-1}	Q_e/mol kg^{-1}	R^2	$k_2 \times 10^3$/mol^{-1} kg min^{-1}	$Hx10^3$/mol kg^{-1} min^{-1}
0.098	0.097	0.970	2910	27
Intraparticle diffusion				
		R^2	$k_i \times 10^3$/mol kg^{-1} $min^{-0.5}$	–
–	–	0.970	2.14	–

distribution coefficients (K_D) were derived from Eq. 12; [38, 39].

$$K_D = \frac{Q}{C_e} \tag{12}$$

The free energy of adsorption ($\Delta G°$) is related to K. Thus, Eq. 13 may be written as;

$$\Delta G = -RT\ln K_D \tag{13}$$

The value of enthalpy changes ($\Delta H°$) and entropy changes ($\Delta S°$) for adsorption was calculated using Eq. 14 in below;

$$\ln K_D = \frac{\Delta S°}{R} - \frac{\Delta H°}{RT} \tag{14}$$

Thermodynamic parameters ($\Delta H°$ and $\Delta S°$) are obtained from Fig. 11. The slope ($-\Delta H°/R$) and y-intercept ($\Delta S°/R$) of the data plotted as $\ln K_D$ against $1/T$. Gibbs free energy change was calculated using Eq. 15.

$$\Delta G° = \Delta H° - T\Delta S° \tag{15}$$

Gibbs free energy change was calculated as -8.8 kJ mol^{-1}, -8.9 kJ mol^{-1} and -9.0 kJ mol^{-1} at 278 K, 298 K and 313 K respectively. The negative $\Delta G°$ indicates that spontaneous nature of adsorption is possible. The $\Delta H°$ value was determined as -8.3 kJ mol^{-1}, indicating that the UO_2^{2+} adsorption on PAA-D process was exothermic at the working temperature. $\Delta S°$ was found as 2.1 J mol^{-1} K^{-1}, which indicates that an increase in the randomness of the adsorbent/solution interface in the adsorption process.

Recovery

The stability of adsorption/desorption is very important with regards to practical use of absorbent. A series of desorption experiments with 1 M HCl, 1 M NaOH, 1 M HNO_3 and 1 M Ethyl alcohol were studied for evaluation of the recovery

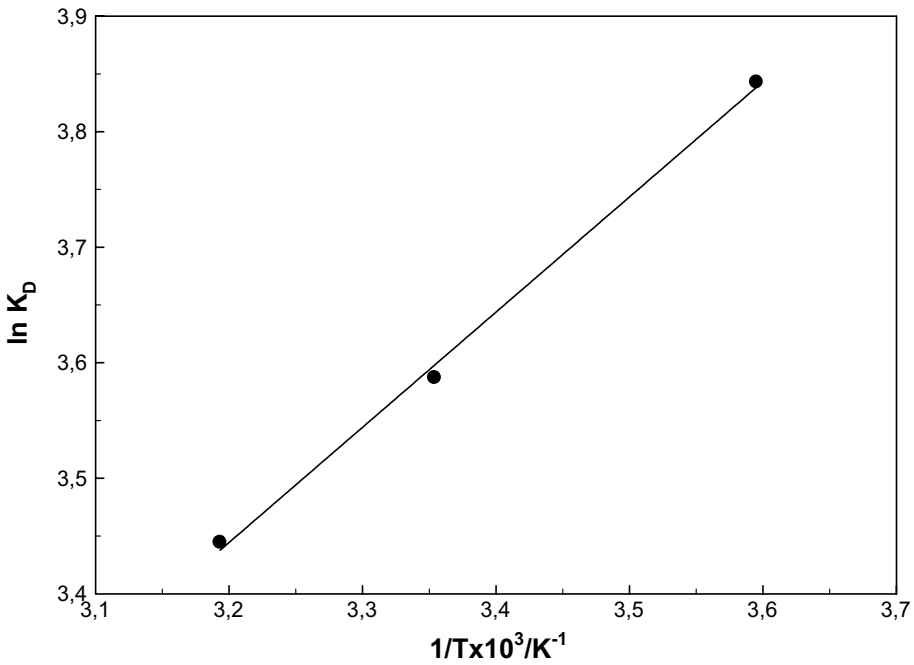

Fig. 11 The effect of temperature on the adsorption {$[UO_2^{2+}]_0$: 1000 mg L^{-1}, adsorbent dosage: 100 mg, natural pH: 4.0–4.5, contact time: 24 h, temperature: 298 K}

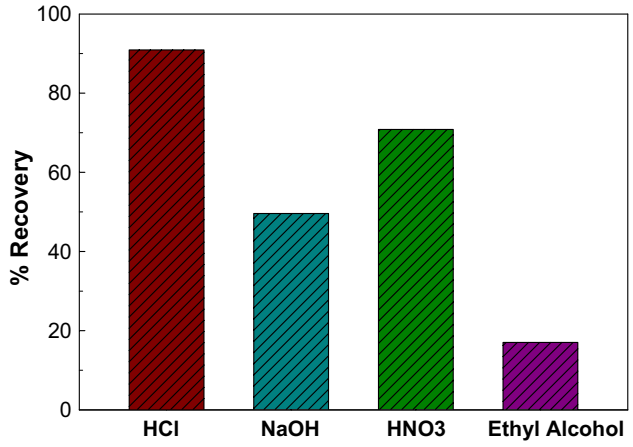

Fig. 12 Recovery percent of various solvent for desorption of uranyl ions {$[UO_2^{2+}]_0$: 1000 mg L^{-1}, adsorbent dosage: 100 mg, natural pH: 4.0–4.5, contact time: 24 h, temperature: 298 K}

conditions for adsorption of UO_2^{2+} onto PAA-D. Results of this study were illustrated in Fig. 12. As can be seen from the Fig. 10, the highest recovery was obtained HCl (91%) and HNO_3 (71%) solutions. Recovery value obtained for the Ethyl alcohol was too low.

Table 4 Adsorption capacity of UO_2^{2+} by various diatomite based adsorbents

Adsorbent	Uptake	References
HDTMA-diatomite	667.40 µmol/g	[17]
Raw diatomite	25.63 µmol/g	[17]
Methylimidazolium modified diatomite	86.78 mg/g	[40]
Magnesium silicate/diatomite	34.54 mg/g	[41]
DT-HDTMA	38.47 mg/g	[42]
Modified diatomite	3.36 mg/g	[43]
Calcined diatomite	0.0081 mmol/g	[44]
Polyacrylamide-diatomite	0.085 mol/kg	This study

Comparison of adsorption capacity of the PAA-D composite with literature

A comparison of the maximum adsorption capacity (X_m) for other low-cost adsorbents and PAA-D-uranyl reported in the literature is presented in Table 4. As shown in this table, the maximum adsorption capacity of PAA-D is higher than most adsorbents.

Conclusion

In this study, batch adsorption tests were performed for the removal of UO_2^{2+} from the aqueous solution using PAA-D composite. Our results obtained can be summarized as follows:

1. Optimal working parameters for maximum adsorption are summarized as follows;
   - The pH of the solution was natural pH:4.0–4.5
   - The adsorbent amount was 100 g
   - The contact time was 24 h and the temperature was chosen as 298 K.
2. The obtained experimental data were fitted to Langmuir, Freundlich and D–R isotherm models. Based on R^2 value obtained, the best explanation for adsorption of UO_2^{2+} on PAA-D was fitted with Freundlich model. The monolayer adsorption capacity was found 0.085 mol kg^{-1} in optimal conditions. Adsorption free energy, which calculated from D–R isotherm was found as E_{DR} (16.2 kJ mol^{-1}). Thus, the obtained results showed that is based on chemical interactions by using ion-exchange mechanism.
3. The adsorption kinetic of UO_2^{2+} ions on PAA-D was explained with pseudo second order model. Kinetic data were best interpreted by a pseudo second order model.
4. Thermodynamic parameters ΔH°, ΔS° ve ΔG° showed that adsorption was exothermic, convenient and spontaneous, respectively.
5. Recovery studies showed that the highest recovery was obtained with HCl, whereas ethyl alcohol had the lowest.
6. Findings in this paper showed that PAA-D adsorbent can be a low-cost, effective and also performing a considerable high adsorption capacity.

Acknowledgements The present study (Project No: ZARA002) was partly supported by Cumhuriyet University Scientific Research Projects Commission (CUBAP), Sivas in Turkey.

Compliance with ethical standards

Conflict of interest The authors have declared no conflict of interest.

References

1. Keith LS, Faroon OM, Fowler BA (2007) Uranium. In: Berlin M, Zalups RK, Fowler BA (eds) Handbook on the toxicology of metals. Academic Press, Burlington, pp 880–903
2. Wang Y, Chen Y, Liu C, Yu F, Chi Y, Hu C (2017) The effect of magnesium oxide morphology on adsorption of U(VI) from aqueous solution. Chem Eng J 316:936–950
3. Abney CW, Mayes RT, Saito T, Dai S (2017) Materials for the recovery of uranium from seawater. Chem Rev 117:13935–14013
4. Liu Y, Zhao Z, Yuan D, Wang Y, Dai Y, Chew WJ (2018) Fast and high amount of U (VI) uptake by functional magnetic carbon nanotubes with phosphate group. Ind Eng Chem R 57:14551–14560
5. Barron-Zambrano J, Laborie S, Viers P, Rakib M, Durand G (2004) Mercury removal and recovery from aqueous solutions by coupled complexation–ultrafiltration and electrolysis. J Membr Sci 229:179–186
6. Jossa A, Kellera E, Aldera AC, Gobela A, McArdella CS, Ternes T (2005) Siegrist H removal of pharmaceuticals and fragrances in biological wastewater treatment. Water Res 39:3139–3152
7. Sajid M, Nazal MK, Baig IN, Osman AM (2018) Removal of heavy metals and organic pollutants from water using dendritic polymers based adsorbents: a critical review. Sep Purif Technol 191:400–423
8. Uddin MK (2017) A review on the adsorption of heavy metals by clay minerals, with special focus on the past decade. Chem Eng J 308:438–462
9. Liu Y, Zhao Z, Yuan D, Wang Y, Dai Y, Zhu Y, Chew JW (2019) Introduction of amino groups into polyphosphazene framework supported on CNT and coated Fe_3O_4 nanoparticles for enhanced selective U(VI) adsorption. Appl Surf Sci 466:893–902
10. Monier M, Abdel-Latif DA (2013) Synthesis and characterization of ion-imprintedresin based on carboxymethyl cellulose for selective removal of UO_2^{2+}. Carbohydr Polym 97:743–752
11. Li WP, Han XY, Wang XY, Wang YQ, Wang WX, Xu H, Tan TS, Wu WS, Zhang HX (2015) Recovery of uranyl from aqueous solutions using amidoximated polyacrylonitrile/exfoliated Na-montmorillonite composite. Chem Eng J 279:735–746
12. Liao Y, Wang M, Chen D (2018) Preparation of polydopamine-modified graphene oxide/chitosan aerogel for uranium (VI) adsorption. Ind Eng Chem R 57:8472–8483
13. Babel S, Kurniawan TA (2003) Low-cost adsorbents for heavy metals uptake from contaminated water. J Hazard Mater 97:219–243
14. Khraisheh MAM, Al-degs YS, Mcminn WAM (2004) Remediation of wastewater containing heavy metals using raw and modified diatomite. Chem Eng J 99:177–184
15. Al-Ghouti MA, Khraisheh MAM, Ahmad MNM, Allen S (2009) Adsorption behaviour of methylene blue onto Jordanian diatomite: a kinetic study. J Hazard Mater 165:589–598
16. Simşek S, Senol ZM, Ulusoy HI (2017) Synthesis and characterization of a composite polymeric material including chelating agent for adsorption of uranyl ions. J Hazard Mater 338:437–446
17. Sprynskyy M, Kovalchuk I, Buszewsk B (2010) The separation of uranium ions by natural and modified diatomite from aqueous solution. J Hazard Mater 181:700–707
18. Sheng G, Wang S, Hu J, Lu Y, Li J, Dong Y, Wang X (2009) Adsorption of Pb(II) on diatomite as affected via aqueous solution chemistry and temperature. Colloids Surf A Physicochem Eng Aspects 339:159–166
19. Caliskan N, Kul AR, Alkan S, Gokirmak Sogut E, Alacabey I (2011) Adsorption of zinc(II) on diatomite and manganese-oxide-modified diatomite: a kinetic and equilibrium study. J Hazard Mater 193:27–36
20. Yu W, Deng L, Yuan P, Liu D, Yuan W, Liu P, He H, Li Z, Chen F (2015) Surface silylation of natural mesoporous/macroporous diatomite for adsorption of benzene. J Colloid Interface Sci 448:545–552
21. Lin JX, Zhan SL, Fang MH, Qian XQ (2007) The adsorption of dyes from aqueous solution using diatomite. J Porous Mater 14:449–455
22. Chiem LT, Huynh L, Ralston J, Beattie DA (2006) An in situ ATR–FTIR study of polyacrylamide adsorption at the talc surface. J Colloid Interface Sci 297:54–61
23. Bagci C, Kutyla GP, Kriven WM (2017) Fully reacted high strength geopolymer made with diatomite as a fumed silica alternative. Ceram Int 43:14784–14790
24. Mukerabigwi JF, Lei S, Fan L, Wang H, Luo S, Ma X, Qin J, Huang X, Cao Y (2016) Eco-friendly nano-hybrid

superabsorbent composite from hydroxyethyl cellulose and diatomite. RSC Adv 6:31607–31618
25. Jaques BJ, Watkins J, Croteau JR, Alanko GA, Tyburska-Püschel B, Meyer M, Xu P, Lahoda EJ, Butt DP (2015) Synthesis and sintering of UN-UO_2 fuel composites. J Nucl Mater 466:745–754
26. Wang Y, Fan C, Wang H, Wang F, Xu J, Duan P, Zhang Y (2015) Effects of TiO_2 on the sintering densification of UO_2–Gd_2O_3 burnable poison fuel. Ceram Int 41:10185–10191
27. Kumari P, Sharma P, Srivastava S, Srivastava MM (2006) Biosorption studies on shelled *Moringa oleifera* Lamarck seed powder: removal and recovery of arsenic from aqueous system. Int J Miner Process 78:131–139
28. Li Z, Chen F, Yuan L, Liu Y, Zhao Y, Chai Z, Shi W (2012) Uranium(VI) adsorption on graphene oxide nanosheets from aqueous solutions. Chem Eng J 210:539–546
29. Shao L, Zhong J, Ren Y, Tang H, Wang X (2017) Perhydroxy-CB[6] decorated graphene oxide composite for uranium(VI) removal. J Radioanal Nucl Chem 311:627–635
30. Langmuir I (1918) The adsorption of gases on plane surfaces of glass, mica and platinum. J Am Chem Soc 40:1361–1403
31. Freundlich HMF (1906) Over the adsorption in solution. J Phys Chem 57:385–471
32. Helfferich F (1962) Ion exchange. McGraw-Hill, New York
33. Romero-Gonzalez J, Peralta-Videa JR, Rodrıguez E, Ramirez SL, Gardea-Torresdey JL (2005) Determination of thermodynamic parameters of Cr(VI) adsorption from aqueous solution onto *Agave lechuguilla* biomass. J Chem Thermodyn 37:343–347
34. Tseng RL, Wu FC, Juang RS (2010) Characteristics and applications of the Lagergren's first-order equation for adsorption kinetics. J Taiwan Inst Chem Eng 41:661–669
35. Ho YS, McKay G (1999) Pseudo-second order model for sorption processes. Process Biochem 34:451–465
36. Wu FC, Tseng RL, Juang RS (2009) Initial behavior of intraparticle diffusion model used in the description of adsorption kinetics. Chem Eng J 153:1–8
37. Cheung WH, Szeto YS, McKay G (2007) Intraparticle diffusion processes during acid dye adsorption onto chitosan. Bioresour Technol 98:2897–2904
38. Boparai HK, Joseph M, O'Carroll DM (2011) Kinetics and thermodynamics of cadmium ion removal by adsorption onto nano zerovalent iron particles. J Hazard Mater 186:458–465
39. Liu Y, Dai Y, Yuan D, Wang Y, Zou L (2017) The preparation of PZS-OH/CNT composite and its adsorption of U(VI) in aqueous solutions. J Radioanal Nucl Chem 314(3):1747–1757
40. Sprynskyy M, Kowalkowski T, Tutu H, Cukrowska EM, Buszewski B (2015) Ionic liquid modified diatomite as a new effective adsorbent for uranium ions removal from aqueous solution. Colloids Surf A 465:159–167
41. Lu S, Hu J, Chen C, Chen X, Gong Y, Sun Y, Tan X (2017) Spectroscopic and modeling investigation of efficient removal of U(VI) on a novel magnesium silicate/diatomite. Sep Purif Technol 174:425–431
42. Salameh S, Khalili FI, Al-Dujaili AH (2017) Removal of U(VI) and Th(IV) from aqueous solutions by organically modified diatomaceous earth: evaluation of equilibrium, kinetic and thermodynamic data. Int J Miner Process 168:9–18
43. Shuibo X, Chun Z, Xinghuo Z, Jing Y, Xiaojian Z, Jingsong W (2009) Removal of uranium (VI) from aqueous solution by adsorption of hematite. J Environ Radioact 100:162–166
44. Donat R, Cılgı G, Aytas S, Cetisli H (2008) Thermodynamic parameters and sorption of U(VI) on ACSD. J Radioanal Nucl Chem 279:271–280